Comparison of H-mode pedestal characteristics in SAS and open divertor configurations on DIII-D

T.H. Osborne[1], L. Casali[1], H.Y. Guo[1], A.L. Moser[1], M. Shafer[2]

[1] *General Atomics, San Diego, USA*

[2] *Oak Ridge National Laboratory, Oak Ridge, USA*

Introduction: The Small Angle Slot (SAS) divertor installed on DIII-D combines high closure with small incidence angle to achieve detachment over a large part of the SOL at low density [1]. Experiments described here compared the H-mode pedestal characteristics in the SAS configuration to those in an otherwise identically shaped lower single null (LSN) open divertor configuration (Fig. 1) with BxΔB drift both toward and away from the X-point, and with I_P = 1MA, B_T = 2T, q_{95} = 4.6, and neutral beam heating power P = 4MW giving $\beta_N \sim 1.7$. Density scans using D_2 gas injection from an outboard main chamber port covered $0.3 \leq n_e^{PED}/n_{GW} \leq 0.6$, where $n_{GW} = 10^{20}/m^3$. The diagnostics used to produce the kinetic profiles as well as the data analysis methods are described elsewhere [2]. Variations of the pedestal pressure. p^{PED}, with configuration were consistent with the stability constraints of the EPED model [4], however other simplifying assumptions in the model where not consistent with observations and overall the model failed to account for the p^{PED} variation.

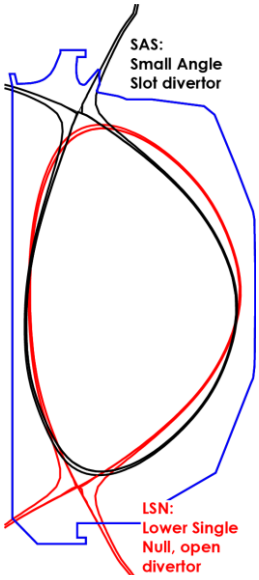

Fig. 1: Matched SAS and LSN shapes

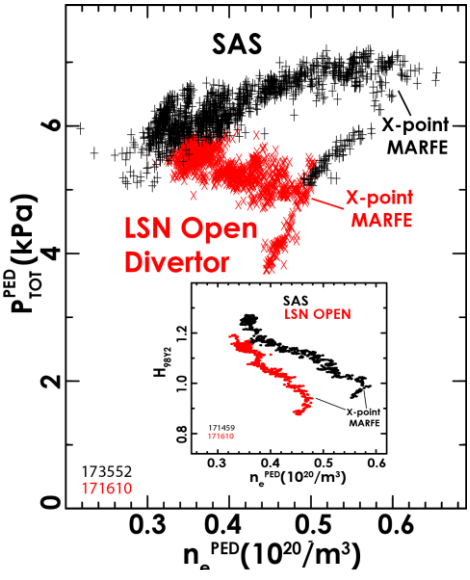

Fig. 2: Comparison of SAS to LSN pedestal pressure versus density for BxΔB away. Insert shows H factor.

Comparison of SAS to LSN with the BxΔB drift away from the X-point: With the BxΔB drift away from the X-point in both configurations, SAS discharges had higher total pedestal pressure, $p_{TOT}^{PED} = p_e^{PED} + p_i^{PED}$, and improved energy confinement enhancement, H_{98Y2}, at a given pedestal density, n_e^{PED} (Fig. 2). A strong decrease in pedestal temperature and pressure above a density where a high radiation zone reached the X-point region was observed in both configurations, although the density at which this occurred was significantly higher for the SAS (Fig. 2). The pedestal profiles for the two configurations at the same n_e^{PED} before MARFE onset in the LSN, corresponding to

conditions just before an ELM, are shown in Fig. 3. The T_e pedestal is narrower at fixed gradient and the n_e pedestal is somewhat narrower and steeper and T_i is reduced producing a significantly lower p^{PED} in the open divertor. The higher pedestal T_e and T_i in the SAS discharge propagate to the axis resulting in higher overall stored energy. A narrowing of the pedestal T_e width along a relatively fixed gradient and a reduction in T_i occurs for both the SAS and LSN discharges as n_e^{PED} increases, although the relationship between the SAS and LSN profiles persists. MHD equilibria were computed using the pressure profiles of Fig. 3 and current density profile set by MSE measurements in the core and a combination of Ohmic, neutral beam driven, and bootstrap current computed with NEO[3] in the pedestal. The pedestal pressure and current density were then varied independently to generate a grid of equilibria on which the ELITE code was run to compute the stability threshold for peeling-ballooning modes, PBM. As is seen in many other experiments, the pedestal reaches the PBM threshold just before an ELM (fig 4). Both the SAS and open divertor are toward the ballooning branch but near the transition between peeling and ballooning with most unstable toroidal mode numbers of 25 and 35 respectively. Here the stability threshold is set as the point when the growth rate exceeds the diamagnetic stabilization level as computed from BOUT++ simulations in [4]. We also compare the measured pedestal pressure to that predicted by the EPED model [4]. Under this model the kinetic ballooning mode, KBM, is taken to limit the pedestal pressure gradient between ELMs with pedestal pressure just before an ELM set by the point where the PBM threshold is crossed. The KBM constraint can be shown to reduce to a relation between the pressure height and width of the form $w \propto (\beta_{POL}^{PED})^{1/2}$ where β_{POL}^{PED} is the pedestal poloidal β, and w is the pressure width in normalized poloidal flux coordinates. The proportionality constant of the relation predicted by theory is in rough agreement with a valued determined empirically from a database of DIII-D equilibria, and the relation $(w_{ne} + w_{Te})/2 = 0.076(2\beta_{POL}^{e\,PED})^{1/2}$ combined with the PBM threshold has been

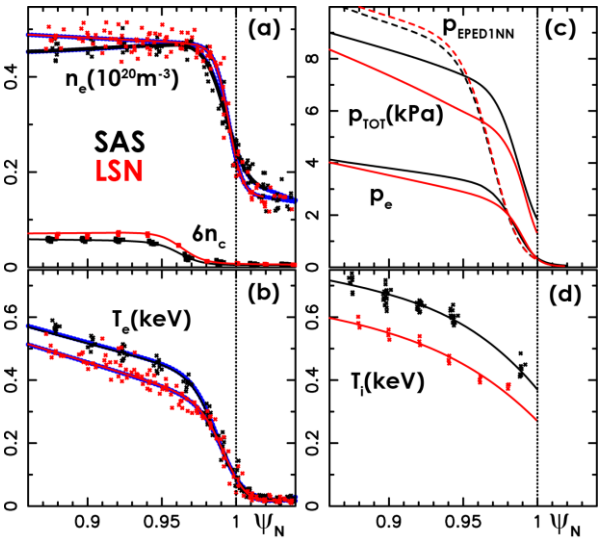

Fig. 3: Experimental pedestal profiles and EPED1NN predicted pressure for SAS and LSN open divertor discharges of Fig. 2.

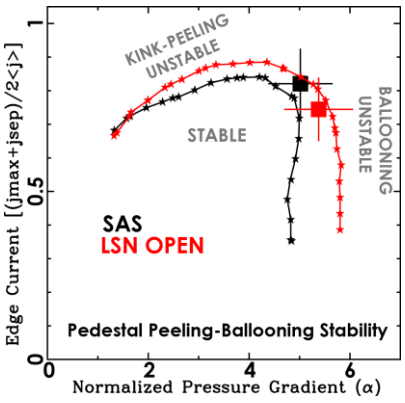

Fig. 4: Pedestal peeling-ballooning stability boundary and experimental values from profiles of Fig.3.

show to predict the pedestal pressures over a wide range of experiments to an accuracy of ±20%. A number of assumptions are normally made in EPED in the relationship between the pedestal profiles and in the equilibrium shape in order to reduce the number of required inputs for a prediction of the pedestal pressure to n_e^{PED}, I_P, B_T, β_N, Z_{EFF}, a, R, triangularity, and elongation: 1) T_i=T_e, 2) Z_{EFF} does not vary in space, 3) n_e and T_e maximum gradient points are aligned, 4) n_e and T_e pedestals have the same width, 5) the separatrix is located at ½ the width out from the T_e maximum gradient point, 6) $n_e^{PED}/n_e^{SEP} = 4$. Also simplified limiter equilibria are used as well as a simplified form for the PBM stability threshold of $\gamma/(\omega_{*i}/2) = 1$. The pedestal pressure prediction of a neural-net version of this usual form for the EPED model trained on DIII-D data[5], designated $P_{EPED1NN}$, is compared to experimental total pedestal pressure in the different divertor configurations in Fig. 3c. The EPED1NN prediction significantly exceeds the measured pedestal pressure particularly for the LSN discharge and the difference in pedestal pressure structure is evident. To test whether the KBM+PBM constraints of EPED are setting the pedestal pressure subject to the effects of the divertor configuration on the relationship between the pedestal profiles, a different approach to applying the model was taken. In this approach, the experimental pedestal T_e and T_i profiles were scaled keeping n_e , Z_{EFF} and the overall stored energy fixed. For each resulting pedestal pressure the width of all profiles were adjusted together by compressing or expanding against the separatrix until the KBM constraint was met. These modified profiles were then used to compute an equilibrium with shape matching the experiment that was tested for PBM stability including the corrected level of diamagnetic stabilization. As seen in Fig. 4, the pedestal is at the PBM stability limit just before an ELM. Overlaid as blue dotted lines with the T_e and n_e profiles in Fig.3(a,b) are the KBM scaling profiles computed using the measured pedestal pressure. These are essentially identical to the fitted experimental profiles. Thus, there is good agreement between the EPED KBM+PBM constraints and the pedestal pressure if the experimental relationship between all the profiles, the full equilibrium shape, and the corrected level of diamagnetic stabilization is included. A more extensive comparison of the two approaches to the EPED model is made in the next section.

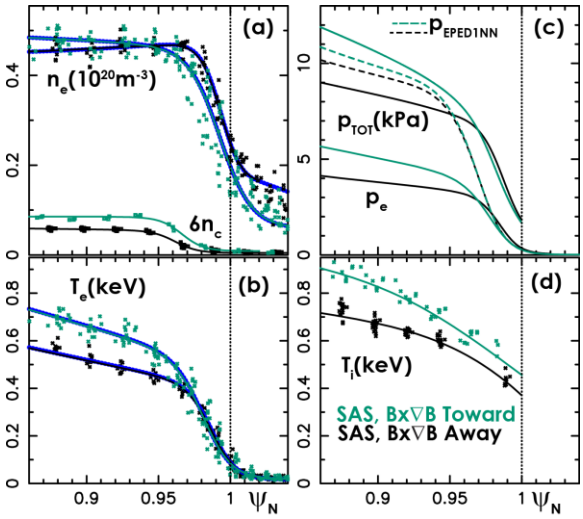

Fig. 5: Pedestal profiles for SAS discharges with different BxVB drift directions

Comparison of SAS to LSN with the BxΔB drift toward the X-point: In contrast to the results in the other drift direction, with the BxΔB drift toward the X-point the SAS and open divertor have similar pedestal structure. The pedestal pressure at a given n_e^{PED} for the SAS discharge with BxΔB drift toward the X-point is significantly higher than in the other drift direction (Fig. 5). Moreover, the reason for this difference is similar to that shown for the SAS and LSN in Fig. 3. In the SAS discharge with BxΔB drift away, the T_e pedestal is narrower along a fixed gradient, n_e is shifted outward and T_i is lower. In the favourable drift direction, the pedestal pressure is close to the EPED1NN prediction although the overall structure is much different (Fig. 5c). Again, there is a close match between the KBM constraint and the measured profiles (blue dotted line in Fig 5a,b). Fig. 6 shows a comparison of the EPED predictions to the measured pedestal pressure over the full n_e^{PED} range. Although the EPED1NN model does not account for the pressure variations (circular points in Fig. 6), good agreement is found applying the KBM+PBM constraints if the experimental relation between the profiles, the actual equilibrium shape, and the corrected diamagnetic stabilization model is used (stars and denoted EPED in Fig. 6).

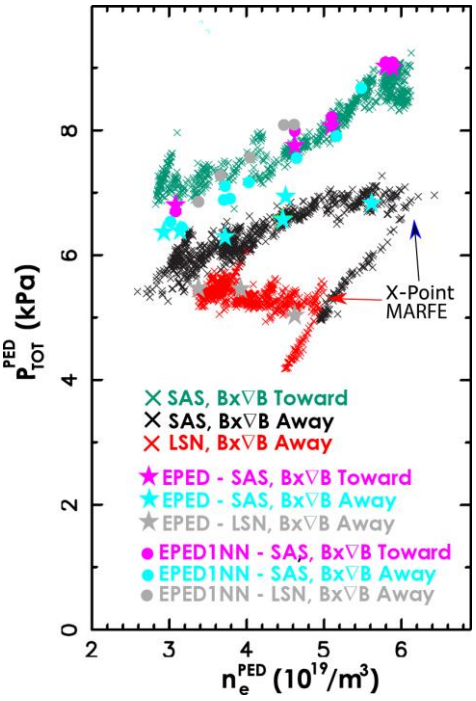

Fig. 6: Comparison of measured pedestal pressure to EPED

Discussion: The KBM+PBM constraints embodied in the EPED model can account for the pressure variation with divertor configuration and density in these experiments if the experimental relation between the pedestal profiles, the full equilibrium shape, and the corrected PBM diamagnetic stabilization model is used. However, a fully predictive model will require a better understanding of the transport processes and sources creating these profile relationships.

This material is based upon work supported by the U.S. Department of Energy, Office of Science, Office of Fusion Energy Sciences, using the DIII-D National Fusion Facility, a DOE Office of Science user facility, under Awards DE-FC02-04ER54698 and DEAC05-00OR22725.

[1] H.Y. Guo, et al., *accepted for publication* Nucl. Fusion (2019).

[2] T.H. Osborne, et al., Nucl Fusion **55** (2015) 063018

[3] E.A. Belli, et. Al., Plasma Phys. Contr. Fusion **56** (2014) 045006

[4] P.B. Snyder, et al., Nucl. Fusion **51** (2011) 103016

[5] O. Meneghini, et al., Nucl Fusion **57** (2017) 086034